Received January 2003
Revised August 2003
Accepted September 2003

Molecular dynamics simulation of micro-Poiseuille flow for liquid argon in nanoscale

J.L. Xu, Z.Q. Zhou and X.D. Xu
Guangzhou Institute of Energy Conversion, Chinese Academy of Sciences, Guangzhou, People's Republic of China

Keywords *Liquid flow, Simulation, Gases*

Abstract *The molecular dynamics simulation of micro-Poiseuille flow for liquid argon in nanoscale was performed in non-dimensional unit system with the control parameters of channel size, coupling parameters between solid wall and liquid particles, and the gravity force. The molecular forces are considered not only among the liquid molecules, but also between the solid wall and liquid molecules. The simulation shows that a larger gravity force produces a larger shear rate and a higher velocity distribution. In terms of the gravity force, there are three domain regions each with distinct flow behaviors: free molecule oscillation, coupling and gravity force domain regions. Stronger fluid/wall interactions can sustain a larger coupling region, in which the flow is controlled by the balance of the intermolecular force and the gravity force. Strong surface interaction leads to small slip lengths and the slip lengths are increased slightly with increasing the shear rate. Weak surface interaction results in higher slip lengths and the slip lengths are dramatically decreased with increasing the shear rate. The viscosities are nearly kept constant (Newton flow behavior) if the non-dimensional shear rate is below 2.0. At higher non-dimensional shear rate larger than 2.0, the viscosities have a sharp increase with increasing the shear rate, and the non-Newton flow appears.*

Nomenclature

A	= slab area by L_xL_y	J_N	= parameter averaging starts from J_N time step
a	= acceleration	J_M	= parameter averaging stops at J_M time step
$F_{s,ij}$	= shifted force between particle i and j	k_B	= Boltzmann's constant
$F^*_{gravity}$, $F^*_{intermolecular}$	= non-dimensional gravity force and intermolecular force	L_x, L_y, L_z	= length of calculation domain in x, y and z coordinates
ΔF_{ij}	= magnitude of the shift force at the cut-off distance	L_s	= slip length at the wall surface
g	= "gravity" acceleration	m	= mass of an argon atom
$H_n(z_i)$	= function defined in equation (12)	N	= total number of fluid particles in the calculation domain (box)
i	= particle i	N_w	= total number of solid particles of both top and bottom walls
$\vec{i}$	= unit vector in axial coordinate	n	= nth slab
j	= particle j	r	= vector coordinate from particle i to particle j
j_w	= solid particle j_w		

The authors would like to thank the National Natural Science Foundation of China with the contract number 10272102 for the financial support.

International Journal of Numerical Methods for Heat & Fluid Flow
Vol. 14 No. 5, 2004
pp. 664-688

0961-5539
DOI 10.1108/09615530410539973

r_c = cut-off distance between two fluid particles
r_{ij} = distance between particle i and j
r_{ij_w} = distance between particle i and solid particle j_w
r_{cw} = cut-off distance between fluid particles and solid wall particles
$\vec{\mathbf{R}}$ = position vector
T = temperature
T_w = wall temperature
T_{fluid} = fluid temperature
t = time
u = average velocity
u_w = fluid velocity at the wall surface
V = potential
V_s = shifted potential
v_x, v_y, v_z = fluid velocity in x-, y- and z-direction
$v^x_{i,j}, v^y_{i,j}, v^z_{i,j}$ = velocity of particle i at the jth time step in x-, y- and z-coordinates
x, y, z = coordinates in x-, y- and z-direction
Δz = slab width in z direction
Δt = time step
ρ = fluid particle number density
ρ_{wf} = solid wall particle number density
ε = energy scale of the fluid particle
ε_{wf} = energy scale between fluid and solid particles
σ = length scale of the fluid particles
σ_{wf} = length scale between fluid and solid particles
η = defined in equation (24)
τ = characteristic time of fluid particles
τ_w = wall shear stress
μ = fluid viscosity at the wall surface
ψ_G, ψ'_G, ψ = random numbers defined in equation (8)

Superscripts

* = non-dimensional parameters defined in equation (19)

1. Introduction

Generally, microelectromechanical system (MEMS) refers to devices having the characteristic length larger than 1 μm but less than 1 mm, that combine electrical and mechanical components, using fabrication process of surface micromachining, bulk micromachining, molding, embossing, etc. In this size range, micromachines have a higher surface to volume ratio, which is one of the advantages to be applied in the compact heat exchangers for the electronic cooling. Single-phase or double-phase microchannel heat exchangers have been proved to be efficient in the development of high power density electrical devices. Another application is driven by the biological and chemical industries. The primary advantage satisfies the scale requirement of biological structures and has the potential to place multiple functions for chemical analysis on a small area. Especially, microvalves, micropumps, microseparations, etc. have been fabricated to transport the biological materials such as proteins, DNA, cells, or to transport the chemical samples.

Heat and fluid flow in microchannels are quite different from those in macrochannels. Owing to the high surface to volume ratio, surface affects domain in small devices. The non-slip boundary conditions, which exist in macroscale, are no longer valid in small scale devices, under some circumstances. Slip flow, thermal creep, rarefaction, viscous dissipation, compressibility effects may have to be taken into account (Gad-el-Hak, 1999).

Engineers should be careful to select the suitable model to predict the microdevices. Also, due to the microsize, there is a very high shear rate across the channel wall. Fluids that are Newtonian at normal shear rate in macrochannels, may become non-Newtonian at extremely high shear rate. The pressure gradient becomes large and was observed to be non-constant in long microducts.

In recent years, many researchers deal with gas flow in microchannels. Knudsen number which is defined as the gas mean free path divided by the channel dimension, is used to characterize the gas flow in microchannels. The Knudsen number regimes were developed by Gad-el-Hak (1999) to decide which model should be used to compute the gas flow in a microdevice. Generally, there are four regimes which are summarized in Table I.

Readers who are interested in the gas flow in microchannels may read the recent review article by Rostami *et al.* (2002).

Compared with gas flow in microchannels, liquid flow in microdevices is a difficult task to be done. There is little analytical or numerical work on liquid flow in microchannels. Some studies involve the experimental measurements. However, due to the difficulties in instrumentation, the data are scattered and have low accuracy. There is no clear conclusion that can be drawn on the liquid flow in microchannels. Liquids have the densities which are about one thousand times of the gases. Molecules are packed with each other more closely. Molecular effects are difficult to compute in liquids because the transport theory is less well-established than the kinetic theory for the gases. In dilute gases, intermolecular forces have little effect on the transport process. The molecules spend most of the time in free flight between the collisions. The random molecular motions are responsible for the gaseous transport process. However, liquids are closely packed with each other and they are always in a collision state. When we apply a shear force, a velocity gradient must be created so that molecules will move relative to one another. On an average, the sum of all intermolecular forces must balance the imposed shear (Gad-el-Hak, 1999).

Molecular dynamics (MD) simulation is one of the effective tools to conduct the liquid flow in microchannels. Kopiik *et al.* (1989) conducted the MD

Euler equations neglecting molecular diffusion	$\mathrm{Kn} \to 0$
Navier-Stokes equations with non-slip boundary conditions	$\mathrm{Kn} \leq 10^{-3}$
Navier-Stokes equations with slip boundary conditions	$10^{-3} \leq \mathrm{Kn} \leq 10^{-1}$
Transition regime	$10^{-1} \leq \mathrm{Kn} \leq 10$
Free molecule flow	$\mathrm{Kn} > 10$

Source: Gad-el-Hak (1999)

Table I.
Gas flow regimes in microchannels

simulation to investigate the microscopic aspects of several slow viscous flows past a solid wall. It is found that systems including several thousand molecules can exhibit reasonable continuum behavior. For Couette and Poiseuille flow, the non-slip boundary condition occurs naturally as a consequence of molecular roughness, the velocity profiles agree with the solutions of the Navier-Stokes equations. The slip boundary condition occurs at lower particle densities. The conclusion can be correct only if one neglects the fluid/wall interactions. Liem *et al.* (1992) performed the investigation of the homogeneous-shear non-equilibrium MD for a simpler solid-liquid interaction. The calculation domain consists of three regions: the top solid wall region, the fluid molecule region and the bottom solid wall region. The particles at the wall boundaries are assumed to be exactly the same as those in the fluid, the same potential acts among all the particles including the wall layers. The boundary particles, however, are subjected to an additional harmonic potential. Because they treated the solid wall particles just as the fluid molecules, the calculation results lead to non-slip solution. In fact, liquid flow in microchannels depends on the fluid molecules themselves, the wall material, and the coupling parameters such as length scale and energy scale between the fluid molecules and the wall particles. Thompson and Robbins (1990) reported MD simulations of Lennard-Jones liquids sheared by two solid walls. They found that slip was directly related to the amount of structure induced in the fluid by the periodic potential from the walls. Slip occurred when there is a weak interaction between the fluid and the solid wall molecules. Later Thompson and Troian (1997) performed the MD simulation of the Couette flow for the unit cell measured $12.51\sigma \times 7.22\sigma \times h$ where h varied from 16.71σ to 24.57σ corresponding to about 1,000 liquid molecules. The velocity profiles in non-dimensional unit was plotted against the non-dimensional length for different wall-fluid coupling parameters. Both slip and non-slip phenomena were observed. The slip length was found to have a sharp increase at higher shear rate, and the non-dimensional viscosities nearly keep constant over a wide range of shear rate.

We presented the study on micro-Poiseuille flow confined between two molecular walls in nanoscale. The flow is induced by applying a uniform acceleration parallel to the walls, as if the liquid were falling under gravity. The problem is similar to the case where the flow is created by the applied pressure drop along the flow direction. The objective of the study is summarized as follows.

- In terms of classical fluid mechanics theory in macroscale, the non-slip boundary conditions always exist. The flow field is not influenced by the solid wall parameters. However, such non-slip boundary is quite questionable in nanoscale due to the solid-liquid force interactions. Such slip boundary and the corresponding flow filed rely on the channel size, coupling parameters between the solid wall and the liquid itself, and the

applied force, or the pressure drop. The main objective of this report is to examine how the slip boundary and the flow field are affected by the above parameters.

- We applied a wide range of the non-dimensional gravity force to produce a wide range of corresponding shear rate, so as to examine how the flow field is influenced by the shear rate, and examine how the transition from Newton flow to non-Newton flow is created.
- We performed the MD simulation with different liquid molecule numbers, to identify how the flow is affected by the channel size.

2. Mathematical models

2.1 Shifted force and potential

Consider Figure 1, the distance of two parallel walls is L_z. The flow field is well established by applying the liquid molecular body forces, as if they were falling under gravity. We select the calculation domain of the box containing N liquid molecules with the three lengths of L_x, L_y and L_z. The periodic boundary conditions are applied in x and y directions. Any liquid particle i in the box has the force interaction with liquid particle j inside the box (j should include all the liquid particles except particle i), and with the wall molecule j_w (j_w is from

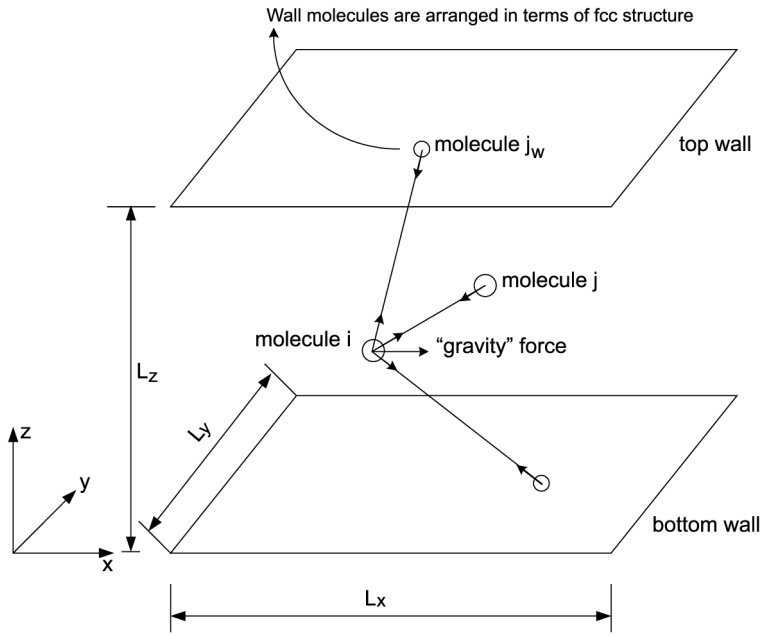

Figure 1.
Diagram of the calculation domain

1 to N_w). In addition to these, the liquid molecule also has the body force as $mg\vec{i}$ (here $\vec{i}$ is the unit vector coordinate in x-direction). Specifically, the simple Lennard-Jones pairwise potential among argon molecules is written as

$$V(r) = 4\varepsilon\left[\left(\frac{\sigma}{r}\right)^{12} - \left(\frac{\sigma}{r}\right)^{6}\right] \tag{1}$$

Based on the work of Haile (1992), the pairwise interaction shifted force between molecule i and j can be written as

$$\vec{F}_{s,ij} = \begin{cases} -\frac{dV_s(r)}{dr}\frac{\vec{r}_{ij}}{|r_{ij}|} = -\frac{dV(r)}{dr}\frac{\vec{r}_{ij}}{|r_{ij}|} + \Delta F_{ij}\frac{\vec{r}_{ij}}{|r_{ij}|} & \text{if } r < r_c \\ 0 & \text{if } r \geq r_c \end{cases} \tag{2}$$

where ΔF_{ij} is the magnitude of the shift force at the cut-off distance r_c.

$$\Delta F_{ij} = -F_{ij}(r_c) = \left.\frac{dV(r)}{dr}\right|_{r_c} \tag{3}$$

The shifted potential $V_s(r)$ corresponding to $F_s(r)$ can be derived from

$$\int_0^{V_s} dV_s = -\int_\infty^r F_s(r)dr \tag{4}$$

Substituting equation (2) into (4) and integrating equation (4) gives

$$V_s(r) = \begin{cases} V(r) - V(r_c) - (r - r_c)\left.\frac{dV}{dr}\right|_{r_c} & \text{if } r < r_c \\ 0 & \text{if } r \geq r_c \end{cases} \tag{5}$$

At this shifted potential, the shifted force between two argon molecules i and j is

$$F_s(r) = \begin{cases} 24\frac{\varepsilon}{\sigma}\left[2\left(\frac{\sigma}{r}\right)^{13} - \left(\frac{\sigma}{r}\right)^{7} - 2\left(\frac{\sigma}{r_c}\right)^{13} + \left(\frac{\sigma}{r_c}\right)^{7}\right] & \text{if } r < r_c \\ 0 & \text{if } r \geq r_c \end{cases} \tag{6}$$

The Lennard-Jones potential interaction between argon molecule and wall molecules has the similar expression except that we use the coupling length scale of σ_{wf} and energy scale of ε_{wf}. Therefore, applying Newton's second law, the acceleration of the argon molecule i in the calculation domain is expressed as

$$24\frac{\varepsilon}{\sigma}\sum_{j\neq i,j=1}^{N}\left[2\left(\frac{\sigma}{r}\right)^{13}-\left(\frac{\sigma}{r}\right)^{7}-2\left(\frac{\sigma}{r_c}\right)^{13}+\left(\frac{\sigma}{r_c}\right)^{7}\right]\frac{\vec{r}_{ij}}{|r_{ij}|}+$$

$$24\frac{\varepsilon_{wf}}{\sigma_{wf}}\sum_{j_w=1}^{N_w}\left[2\left(\frac{\sigma_{wf}}{r}\right)^{13}-\left(\frac{\sigma_{wf}}{r}\right)^{7}-2\left(\frac{\sigma_{wf}}{r_{cw}}\right)^{13}+\left(\frac{\sigma_{wf}}{r_{cw}}\right)^{7}\right]\frac{\vec{r}_{ij_w}}{|r_{ij_w}|}+m\vec{gi} \quad (7)$$

$$=m\vec{a}$$

where r_c is the cut-off distance between liquid molecule i and j which is set to be 2.5σ, r_{cw} is the cut-off distance between liquid molecule i and the wall particle j_w which is $2.5\sigma_{wf}$.

2.2 Thermal wall model

For any liquid argon particle, it has the force interaction not only between such particle and its neighbor particles, but also between such particles and the solid wall particles. When the liquid particle is close to the solid wall surface, the repulsive force will push the liquid particle away from the wall surface. However, some liquid particles (not all) still have the possibility to collide the wall surface. Therefore, the wall surface barrier should be set to ensure that all the liquid particles are confined between the two wall surfaces. Consider the situation that the liquid particles striking the wall surface, MD simulations applied various types of boundaries (for example, specula surfaces, periodic boundaries and thermal walls). In the present report, the thermal wall models is employed. When a liquid particle strikes a thermal wall at the temperature T_w, all three components of velocities are reset to a biased Maxwellian distribution. The three velocity components after the liquid particles strike the wall surfaces are (Alexander and Garcia, 1997)

$$v_x=\sqrt{\frac{k_B T_w}{m}}\psi_G,$$

$$v_y=\sqrt{\frac{k_B T_w}{m}}\psi'_G, \quad (8)$$

$$v_z=\pm\sqrt{-\frac{2k_B T_w}{m}\ln\psi}$$

The positive sign of v_z is for the liquid particles striking the bottom wall surface, while the negative sign is for the liquid particles striking the top wall surface. ψ is a uniformly distributed random number in (0, 1) and ψ_G, ψ'_G are Gaussian-distributed random numbers with zero mean and unit variance.

When a particle j at time t has just crossed a thermal wall during a time step from $\vec{r}_j(t - \Delta t)$ to a position $\vec{R}$ at time t, the following procedure is activated:

- A new velocity is sampled in terms of equation (8).
- The colliding particle is moving to a new position according to $\vec{r}_j(t) = \vec{R} + \vec{v}\Delta t$ (Figure 2(a)).
- If $\vec{r}_j(t)$ is still beyond the thermal wall, we substitute $\vec{r}_j(t) + \vec{b}$ for $\vec{r}_j(t)$ and $\vec{r}_j(t - \Delta t) + \vec{b}$ for $\vec{r}_j(t - \Delta t)$, where $\vec{b}$ is the difference between $\vec{r}_j(t)$ and its projection on the wall (Figure 2(b)).
- The particle positions which have not crossed the thermal wall are not affected.

The detailed reentry mechanism at the thermal wall is described by Tenenbaum *et al.* (1982), and is shown in Figure 2. Corresponding to Figure 2(a), a particle in A at time $(t - \Delta t)$ is assumed to reach the wall in B in the time interview $(t - \Delta t, t)$, then the thermalization mechanism will bring it in C at time t. Owing to the discreteness of the integration algorithm the particle will be in B' at time t. Thus, the reflection is performed by endowing the particle in B' with the thermal velocity and moving it to C'. C' is the new position at time t, and B' is the (new) position at time $t - \Delta t$. Referring to Figure 2(b), if the

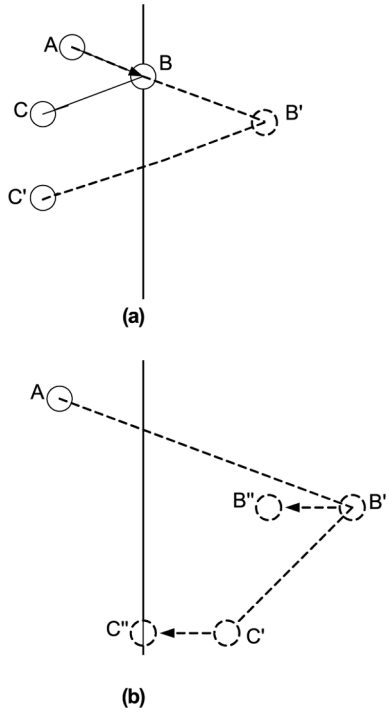

Source: Tenenbaum *et al.* (1982)

Figure 2.
Reentry mechanism at the thermal wall

particle is still beyond the thermal wall after the striking process, it moved to the wall in C'', while the position B' moved by the same amount to B''. C'' is the (new) position at time t, and B'' is the (new) position at time $t - \Delta t$.

Because both the top and bottom walls are not moving, the velocities of wall particles are set to be zero. The particles are fixed in the specified positions in terms of the face-centered-cubic (fcc) structure.

2.3 Initial conditions

To start the finite-difference algorithm, liquid particle positions (x_i, y_i, z_i) and their time derivatives must be assigned at time $t = 0$. The liquid positions should not be assumed randomly because randomly assigned positions will lead to the unphysically large repulsive force that causes the numerical failure of the numerical calculation. Thus, the fcc structure is still applied. However, the fcc structure will be melting when the "gravity" force acts on the liquid particles. At the beginning of the calculation, randomly distributed velocities are assumed to activate the calculation. However, in order to make sure that the steady-state can be easily reached after some reasonable time, the randomly distributed velocities should satisfy the case that the total kinetic temperature is equal to the kinetic energy

$$\frac{3}{2} N k_{\mathrm{B}} T_{\mathrm{fluid}} = \frac{1}{2} m \sum_{i=1}^{N} \left(v_{i,x}^2 + v_{i,y}^2 + v_{i,z}^2 \right) \tag{9}$$

Values for the initial acceleration $a_i(0)$ are determined in terms of the positions $r_i(0)$ by computing the force on each atom and applying Newton's second law. The Gear finite-difference algorithm also needs the higher derivatives. These higher derivatives are assumed to be zero for the initial time step to activate the calculation.

$$\begin{aligned} x_i'''(0) = x_i^{iv}(0) = x_i^{v}(0) = 0 \\ y_i'''(0) = y_i^{iv}(0) = y_i^{v}(0) = 0 \\ z_i'''(0) = z_i^{iv}(0) = z_i^{v}(0) = 0 \end{aligned} \tag{10}$$

2.4 Minimum-image criterion

In MD simulation, the periodic boundary condition and the molecular image forces should be considered. Equation (7) is written for the molecule i interacted with the N molecules in the box and the N_{w} molecules of the top and bottom walls. When Newton's second law is applied to evaluate the molecular interaction for the molecule i, the image force term must be taken into account. For the present application, the first two sum terms of equation (7) are corrected as

$$\vec{F}_{i,\mathrm{s}} = -\sum_{\alpha_x=-1}^{\alpha_x=1}\sum_{\alpha_y=-1}^{\alpha_y=1}\frac{\mathrm{d}V_{\mathrm{s}}(\vec{r}_{ij}-\alpha L)}{\mathrm{d}r_i} - \sum_{\alpha_x=-1}^{\alpha_x=1}\sum_{\alpha_y=-1}^{\alpha_y=1}\frac{\mathrm{d}V_{\mathrm{s}}(\vec{r}_{ij_{\mathrm{w}}}-\alpha L)}{\mathrm{d}r_i} \tag{11}$$

where L is L_x in x-direction and L_y in y-direction. α is the cell translation vector. Equation (11) accumulates forces for molecule i interacted with atom j and its images outside of the box, and the molecule j_{w} of the two walls and its images.

A minimum-image criterion has been developed to perform the real sum of equations (11) and (7). For a cubic container in three dimensions, the minimum image criterion applies separately to each Cartesian component of the pair separation vector. For the x component, we use $x_{ij} \rightarrow x_{ij} - \alpha_x L_x$ where $\alpha_x = 0$ if $-0.5L_x \leq x_{ij} \leq 0.5L_x$, $\alpha_x = -1$ if $x_{ij} \leq -0.5L_x$ and $\alpha_x = 1$ if $x_{ij} \geq 0.5L_x$ (Haile, 1992). Similar procedure was applied for y_{ij}. There is no image effect for the z component.

2.5 Parameter averaging

The Gear finite-difference algorithm for the MD simulation needs a suitable time step, which is chosen from $\Delta t = 0.005\tau$ to 0.0005τ depending on the non-dimensional gravity force, where τ is the Lennard-Jones molecular oscillation time $\tau = \sigma\sqrt{m/\varepsilon}$. For large gravity force (large shear rate), the liquid particle has a small characteristic time. In order to match the small characteristic time resulted from the large gravity force with the molecular oscillation time τ, a small time step was used. For instance, for the non-dimensional gravity force of 5.0, the time step of $\Delta t = 0.0005\tau$ was applied. Much smaller time step results in no change of the flow field. Following the integrated time of 100τ, the system has evolved into the steady-state, the mean flow velocity, temperature were computed as a function of z. The function $H_n(z_i)$ was defined such that

$$H_n(z_{i,j}) = 1 \ \text{ if } \ (n-1)\Delta z < z_i < n\Delta z, \tag{12}$$

otherwise

$$H_n(z_{i,j}) = 0$$

where the subscript j represents the jth time step.

The average non-dimensional number density in the nth slab from time step J_N to time step J_M is

$$\rho\sigma^3 = \frac{\sigma^3}{A\Delta z(J_M - J_N + 1)}\sum_{j=J_N}^{J_M}\sum_{i=1}^{N} H_n(z_{i,j}) \tag{13}$$

where z_i is the coordinate of the mid-point of the nth slab, A is the area expressed as $L_x \times L_y$. J_N and J_M are the start and ending time step of the parameter averaging. The integrated time interval from J_N time step to J_M time

step is larger than 100τ. The slab average velocity from J_N time step to J_M time step is computed as

$$u(z_i) = \frac{1}{(J_M - J_N + 1)\sum_{i=1}^{N} H_n(z_{i,j})} \sum_{j=J_N}^{J_M} \sum_{i=1}^{N} H_n(z_{i,j})\, v_{i,j}^x \tag{14}$$

where $v_{i,j}^x$ is the velocity in x component of particle i at time step j.

When the steady-state is reached, the gravity force of the N liquid particles in the box should be balanced by the wall friction force of the top and bottom walls, therefore, we have

$$2\tau_w L_x L_y = Nmg \tag{15}$$

the fluid viscosity at the wall surface is

$$\mu = \frac{\tau_w}{\left.\frac{du(z)}{dz}\right|_w}, \tag{16}$$

where $du(z)/dz|_w$ is the shear rate at the wall surface.

In terms of classical fluid mechanics theory, the fluid at the wall surface has the same velocity as the wall surface. However, for the present problem in nanoscale, slip at the wall surface may occur. The slip length is defined as "how far the fluid should travel beyond the thermal wall to reach the same velocity as the wall surface". Figure 3 is used to demonstrate the method to obtain the slip length at the wall surface. AB is the straight line which shares the same velocity gradient at point B with that of the curve BC, while curve BC represents the velocity profile across the two walls. At the bottom wall surface at $z = 0$, the axial fluid velocity is u_w (slip flow), thus line AB has the following expression

$$u - u_w = \left.\frac{du}{dz}\right|_w z, \tag{17}$$

finally the slip length is calculated as

$$L_s = \left| \frac{u_w}{\left[\frac{du(z)}{dz}\right]_w} \right| \tag{18}$$

3. Results and discussion

3.1 Non-dimensional unit system

It is noted that equation (7) is written in unit system. However, equation (7) can be converted into the non-dimensional form using the following non-dimensional parameters

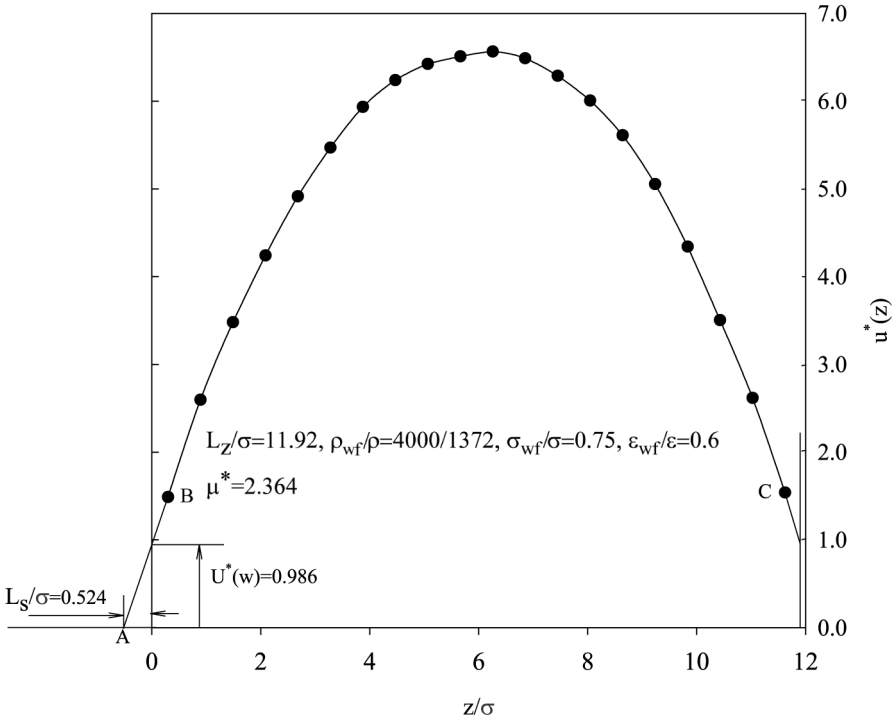

Figure 3.
Method to obtain the slip length in terms of velocity profile

$$r^* = \frac{r}{\sigma}, \quad x^* = \frac{x}{\sigma}, \quad y^* = \frac{y}{\sigma}, \quad z^* = \frac{z}{\sigma}, \quad t^* = \frac{t}{\tau}, \quad F^* = \frac{F\sigma}{\varepsilon},$$
$$v^* = v\sqrt{m/\varepsilon}, \quad a^* = \frac{a}{\sigma/\tau^2} = \frac{\tau^2}{\sigma}a \tag{19}$$

Equation (7) can be rewritten as

$$\vec{a}_i^* = 24\sum_{j\neq i, j=1}^{N}\left(\frac{2}{|r_{ij}^*|^{13}} - \frac{1}{|r_{ij}^*|^7} - \frac{2}{(r_c^*)^{13}} + \frac{2}{(r_c^*)^7}\right)\frac{\left(\vec{r}_i^* - \vec{r}_j^*\right)}{|r_{ij}^*|}$$
$$+ 24\frac{\varepsilon_{wf}/\varepsilon}{\sigma_{wf}/\sigma}\sum_{j_w=1}^{N_w}\left[\left(\frac{\sigma_{wf}}{\sigma}\right)^{13}\frac{2}{|r_{ij_w}^*|^{13}} - \left(\frac{\sigma_{wf}}{\sigma}\right)^7\frac{1}{|r_{ij_w}^*|^7} - \frac{2}{|r_{cw}^*|^{13}} + \frac{1}{|r_{cw}^*|^7}\right] \tag{20}$$
$$\times\frac{\left(\vec{r}_i^* - \vec{r}_{j_w}^*\right)}{|r_{ij_w}^*|} + \frac{m\sigma}{\varepsilon}\vec{gi}$$

The present micro-Poiseuille flow is controlled by the parameters of liquid particle number N, density ratio of solid wall to liquid ρ_{wf}/ρ, length scale ratio of solid wall to liquid σ_{wf}/σ, energy scale ratio of solid wall to liquid $\varepsilon_{wf}/\varepsilon$, and the applied non-dimensional gravity force of $m\sigma(g)/\varepsilon$. Combining equations (15) and (16), the non-dimensional viscosity is computed as

$$\mu^* = \frac{\mu}{\varepsilon\tau\sigma^{-3}} = \frac{\rho\sigma^3 L_z^*}{2\frac{du}{dz}\Big|_w^*}\frac{m\sigma g}{\varepsilon} \tag{21}$$

Note that $\rho\sigma^3$ is the fluid non-dimensional number density and is 0.81 for liquid argon. L_z^* and $du/dz|_w^*$ are the non-dimensional channel length in z direction and the non-dimensional velocity gradient at the wall surface.

In terms of equation (18), the non-dimensional slip length is rewritten as

$$L_s^* = \frac{L_s}{\sigma} = \frac{u_w^*}{\frac{du}{dz}\Big|_w^*} \tag{22}$$

3.2 Verification of the present MD model

As described in Section 1, the previous MD simulation focuses on the dilute gas and the non-slip flow at the wall surface. Very little MD simulation was performed for the liquid flow in microchannels. The present MD simulation for the slip flow confined between two parallel plates was compared with the numerical work by Thompson and Troian (1997). The geometry considered by Thompson and Troian (1997) was the two parallel walls with the bottom one stationary and the top one moving at a given constant speed in axial coordinate. The liquid inside the two plates are sheared by the top solid wall thus the flow field could be established. The calculation domain measured $12.51\sigma \times 7.22\sigma \times h$ where $h = 24.57\sigma$. Both the top and the bottom walls are characterized by the indicated density and Lennard-Jones parameters. Values for ε_{wf}, σ_{wf} and ρ_{wf} are expressed in units of ε, σ and ρ, respectively. The liquid is argon with mass $m = 6.67 \times 10^{-23}$ g, the length scale of $\sigma = 0.34$ nm, and the energy scale of $\varepsilon = 1.67 \times 10^{-21}$ J. The corresponding time scale is $\tau = 2.16 \times 10^{-12}$ s. If one neglects the last term of the right hand side of equation (20) and applies a constant moving speed of the top wall, the present model for the micro-Poiseuille flow can be suitable for the MD simulation of the micro Couette flow as performed by Thompson and Troian (1997). The comparison between the present MD simulation for the Couette flow and the work by Thompson and Troian (1997) is shown in Figure 4. It is shown that they match very well, providing the evidence that the present MD approach is correct, including both of the MD simulation itself, but also the proposed wall/fluid interaction model.

As described in Section 2.1 (thermal wall model), when the liquid particle is close to the wall surface, the repulsive force will push the liquid particle away

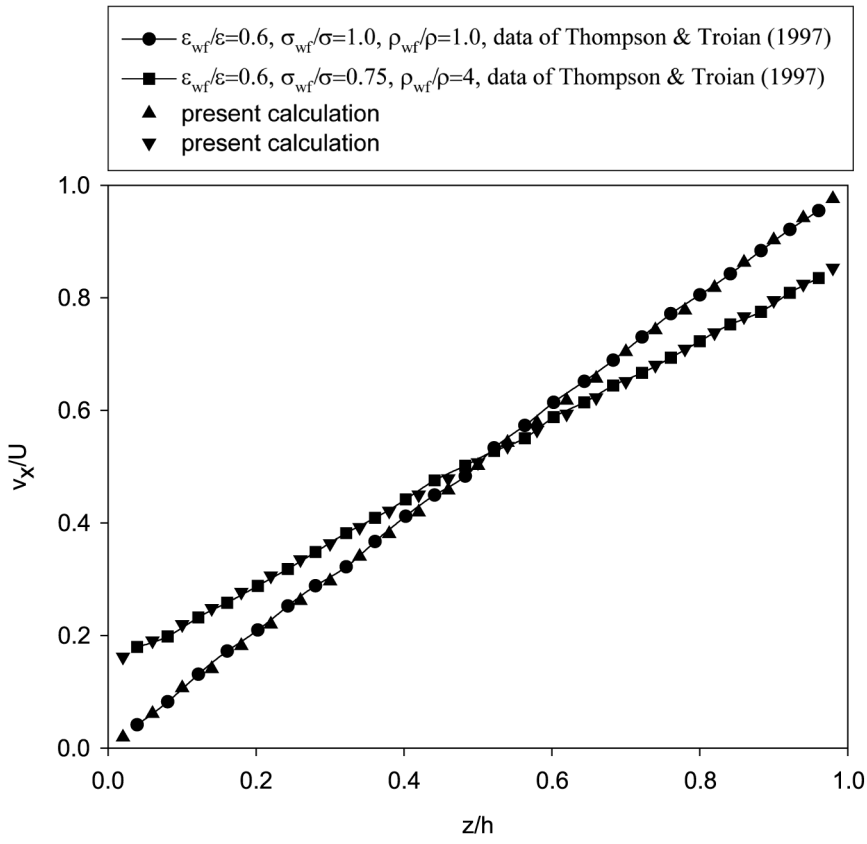

Figure 4.
Comparison of the present calculations with those of Thompson and Troian (1997)

from the wall surface. Theoretically, such repulsive force never lets the liquid particle travel beyond the wall surface. However, in the real computation, we cannot guarantee that no liquid particle would penetrate the wall surface. This is because we cannot use an infinity small time step. By monitoring the calculation process through each time steps, for most of the time step, indeed no liquid particle can exactly reach the wall surface. Accidentally, there are a couple of liquid particles striking the wall. Under such conditions, we incorporate the thermal wall model to ensure that all the liquid particles confined to the two parallel walls. In other words, the thermal wall model was used as the accessorial model. This is the connection between the fluid/wall interaction model and the thermal wall model. Because the fluid/wall interaction mechanism has the domain contribution to the fluid structures near the wall surface, such interaction leads to the slip boundary condition at the wall. The typical velocity profile across the two wall surface is shown in Figure 3 with the slip boundary condition.

3.3 Effect of the gravity force and the coupling parameters

We performed the MD simulation over a wide range of non-dimensional gravity force and coupling parameters between solid and liquid molecules. Most of the numerical work was performed for the liquid calculation domain of 1,372 and 500 fluid atoms. We use the cubic fluid box configuration with the same lengths of L_x, L_y and L_z. Such arrangement results in the length of $L_z = 11.92\sigma$ (4.05 nm) for 1,372 liquid molecules and $L_z = 8.515\sigma$ (2.89 nm) for 500 liquid atoms. With the varying non-dimensional gravity force, it is identified that the flow has three distinct regions as shown in Figure 5, and they are described as follows.

At very small non-dimensional gravity force, for instance, less than 0.1, the flow behaves like free molecular oscillation. In other words, when the gravity potential in terms of the molecular length scale is one order less than the energy scale, the gravity force has no effect on the flow. The liquid molecules oscillate randomly in the three coordinates with the molecular characteristic time scale of τ. The mean flow velocities in all the three coordinates are zero. The system is similarly isolated without any applied force or the pressure gradient. Owing to the described flow behavior, the region was identified as "the free molecular oscillation region".

By increasing the gravity force, for some cases between 0.1 and 10, the flow relies on both the non-dimensional gravity force and the intermolecular force due to the Lennard-Jones potential. The flow behaves like the random molecular oscillation in y- and z-coordinates with zero mean average velocity, but has the net mean average velocity in x-coordinate. The typical mean axial velocity versus z-coordinate has a quadratic function, as shown in Figure 3. However, compared to the classical Poiseuille flow in macroscale, the slip boundary at the solid-liquid interface occurs. The region is named as "the coupling region". The coupling region is the most important one that we discuss in Section 3.4.

Further, by increasing the non-dimensional gravity force, it was found that the intermolecular force had no effect on the mean axial velocity. The mean axial velocity had a uniform distribution across the two channel walls, and had a linear increase with time at a constant acceleration of the non-dimensional gravity force. Typical mean axial velocities versus time are shown in Figure 6.

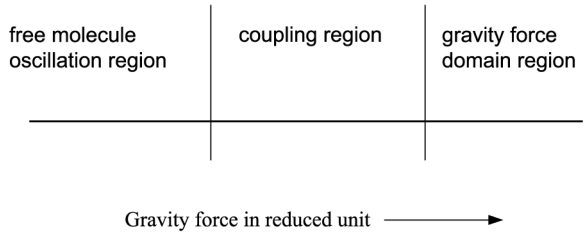

Figure 5.
Three distinct flow regions in terms of applied gravity force

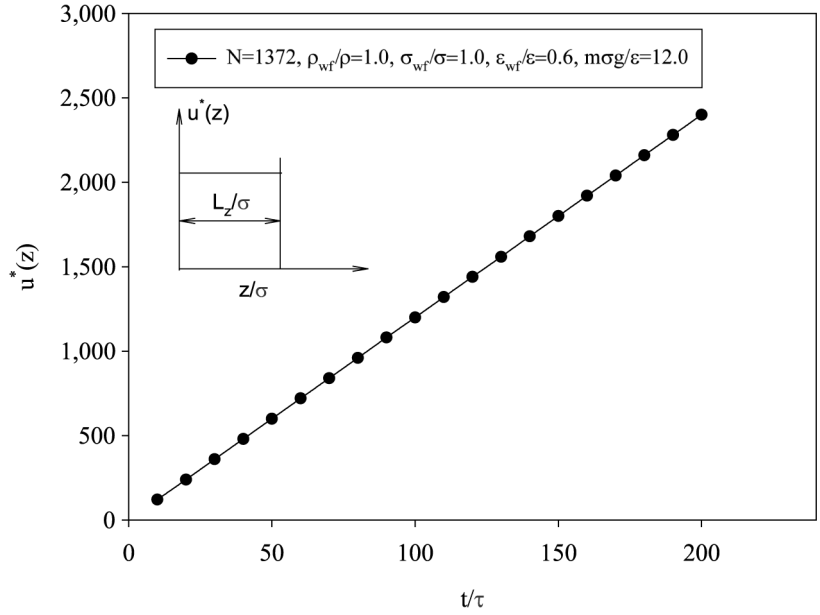

Figure 6.
Mean axial velocity versus time in gravity force domain region

We name this region as the "gravity force domain region". In terms of this, the mean axial non-dimensional velocity can be expressed as

$$u^*(z) = \frac{m\sigma g}{\varepsilon}\frac{t}{\tau} \tag{23}$$

The transitions among the three regions are summarized in Table II.

Comparing cases 1 and 2, we understand that with strong molecular interaction at the fluid/wall interface (case 1), the coupling region can sustain a wide region. Weak interaction at the wall surface for case 2 shows that the transition from the coupling region to the gravity force domain region occurs at a small non-dimensional gravity force. Comparing cases 3, 4 and 5 leads to the same conclusion.

Case no.	Liquid molecule number	ρ_{wf}/ρ	σ_{wf}/σ	$\varepsilon_{wf}/\varepsilon$	Free oscillation region	Coupling region	Gravity force domain region
1	500	1.0	1.0	0.6	$m\sigma g/\varepsilon < 0.1$	$0.1 \le m\sigma g/\varepsilon \le 15$	$m\sigma g/\varepsilon > 15$
2	500	2.74	0.75	0.2	$m\sigma g/\varepsilon < 0.05$	$0.05 \le m\sigma g/\varepsilon \le 11$	$m\sigma g/\varepsilon > 11$
3	1,372	1.0	1.0	0.6	$m\sigma g/\varepsilon < 0.05$	$0.05 \le m\sigma g/\varepsilon \le 10$	$m\sigma g/\varepsilon > 10$
4	1,372	2.92	0.75	0.6	$m\sigma g/\varepsilon < 0.05$	$0.05 \le m\sigma g/\varepsilon \le 3$	$m\sigma g/\varepsilon > 3$
5	1,372	2.92	0.75	0.2	$m\sigma g/\varepsilon < 0.1$	$0.05 \le m\sigma g/\varepsilon \le 2$	$m\sigma g/\varepsilon > 2$

Table II.
Transitions among the three regions for different cases

For the classical Poiseuille flow at the macroscale, the flow field is controlled by the channel size and the applied gravity force, the non-slip boundary condition always exists at the wall surface. However, the present micro-Poiseuille flow is governed by the non-dimensional gravity force, the intermolecular force not only among the liquid particles, but also among the liquid particles and the solid molecules, and the channel size. The above transitions among the free molecular oscillation region, the coupling region and the gravity force domain region are related to the relation of the non-dimensional gravity force to the intermolecular force. We define a non-dimensional parameter which governs transitions such as

$$\eta = \frac{F^*_{\text{gravity}}}{F^*_{\text{intermolecular}}} \tag{24}$$

Because the non-dimensional intermolecular force always has the unit order, η should be close to the non-dimensional gravity force. For small η such as less than 0.05-0.1, the non-dimensional gravity force is so small that the axial flow field could not be established. By increasing the non-dimensional gravity force such as between 0.1 and 10, the flow transfers to the coupling region in which the flow is governed by both the gravity force and the intermolecular force. Further increasing η, the flow is transferred to the gravity force domain region in which only the gravity force has influence on the flow field. The flow transitions among the three regions is similar to that of the classical flow transition from laminar flow to turbulent flow in terms of the Reynolds number, which is defined as the inertia force divided by the viscous force. For small Reynolds number such as less than 2,000, the flow is laminar, while for large Reynolds number the flow is turbulent, and a transition region exists between them.

3.4 Flow behavior in the coupling region

Typical MD simulation results for 1,372 liquid molecules at the non-dimensional gravity force of 0.1 are plotted in Figure 7 against the channel height. Both the number density and the mean axial velocity have a symmetrical distribution about the channel centerline. It is shown that the number densities have peak values near the two wall surfaces. In other words, the liquid molecules near the wall surface are packed much more closely than those far away from the wall surface. Generally, the coupling parameters have little influence on the number density distribution. However, the mean axial velocities are much dependent on the coupling parameters. The stronger fluid/wall interaction (curve dotted by "●") leads to a smaller velocity distribution than those of weak surface interaction (curves dotted by "▪" and "▲"). It is observed that the slip boundary condition occurs for all the cases. However, the slip velocity at the wall surface is very small for the strong fluid/wall interactions, and it is increased by decreasing the interaction

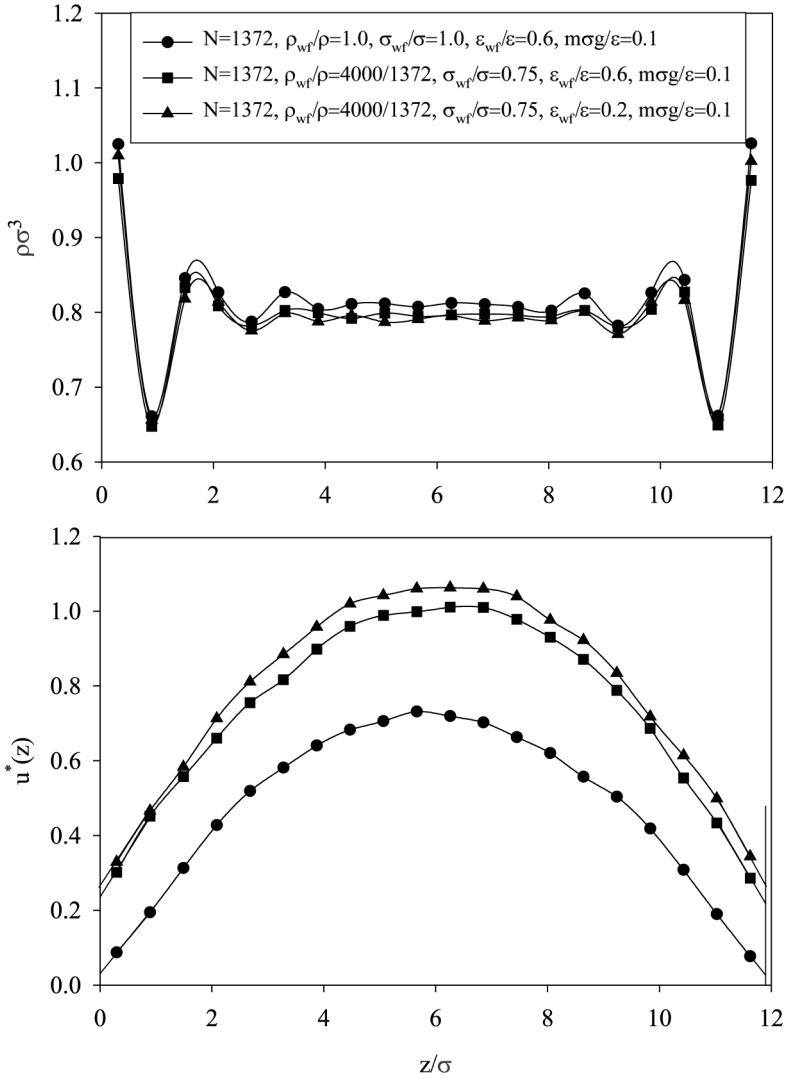

Figure 7.
The number density and mean axial velocity profile in the channel

intensity (increasing ρ_{wf}/ρ, decreasing σ_{wf}/σ and $\varepsilon_{wf}/\varepsilon$). Similar MD simulation results at the non-dimensional gravity force of 2.0 are shown in Figure 8 with a higher mean axial velocity distribution. At higher non-dimensional gravity force, the mean axial velocities show smaller differences for both strong and weak surface interactions.

A certain non-dimensional gravity force produces a corresponding non-dimensional shear rate at the wall surface. Such relationships are demonstrated in Figure 9 for 1,372 liquid molecules at different coupling

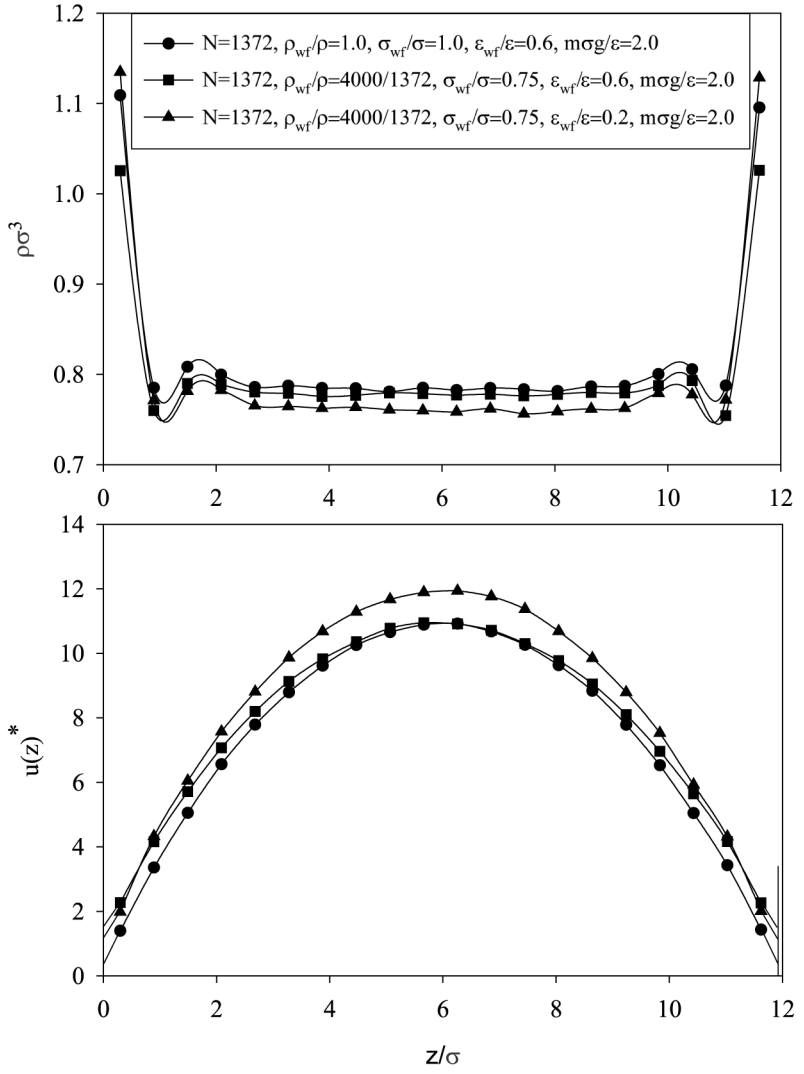

Figure 8.
The number density and mean axial velocity profile in the channel

parameters, indicating that for the weak fluid/wall interactions (curves dotted by "■" and "▲"), the coupling region in which both the intermolecular force and the gravity force act on the flow is much shortened. Surprisingly, it is found that different coupling parameters create similar shear rate at a given non-dimensional gravity force.

The non-dimensional slip lengths and viscosities are shown in Figure 10 versus the non-dimensional shear rate at the wall surface. The slip lengths are very small and has a small increase with increasing the non-dimensional shear rate for strong fluid/wall interactions. However, the weak surface interaction

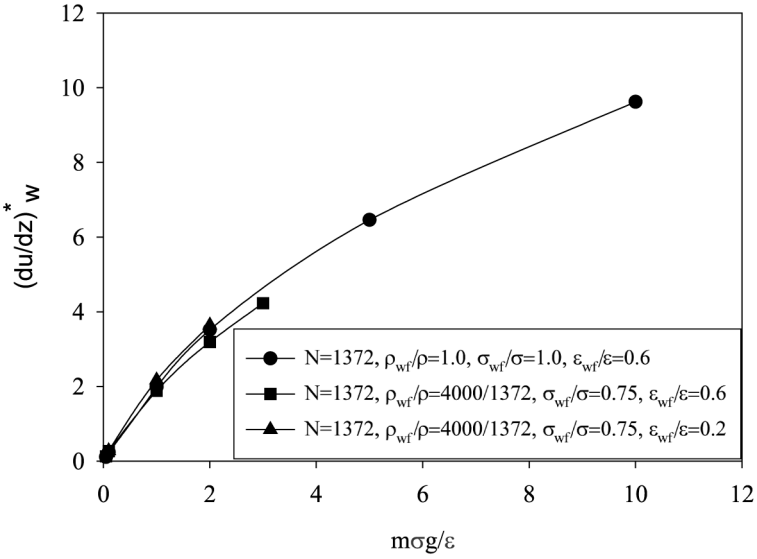

Figure 9.
The non-dimensional shear rate against the non-dimensional gravity force

leads to large slip lengths and such slip lengths are dramatically decreased by increasing the non-dimensional shear rate. It is interesting to note that the non-dimensional viscosities are nearly a constant value of around 2.0 if the non-dimensional shear rate is less than 2.0, leading to the Newton flow behavior. On the other hand, once the non-dimensional shear rate is larger than 2.0, the non-dimensional viscosities have a sharp increase, leading to the non-Newton flow behavior. The three transition points from the Newton to non-Newton flow were identified as (1.992, 2.424), (2.168, 2.227) and (1.883, 2.564). Therefore, it is concluded that the flow characteristics are quite sensitive to the applied shear rate.

3.5 Effect of the liquid particle numbers

The velocity profiles with strong fluid/wall interactions for 500 and 1,372 liquid molecules are shown in Figure 11 against the channel height Larger fluid molecule number (larger channel height) produces much higher velocity distribution. This is because at a larger channel height, the mean axial flow field can be established more easily than that of a small particle number system, and the influence of the fluid/wall interaction can also be decreased for large liquid number system. The similar results are also provided with the weak surface interactions for 500 and 1,372 liquid molecules in Figure 12. Comparing Figures 11 and 12, slight differences were observed on the velocity profile for both strong and weak surface interactions at a given fluid number system. This is because the two figures are plotted for the non-dimensional gravity force of 1.0, such high gravity force plays a major role on the velocity profile development in the channel.

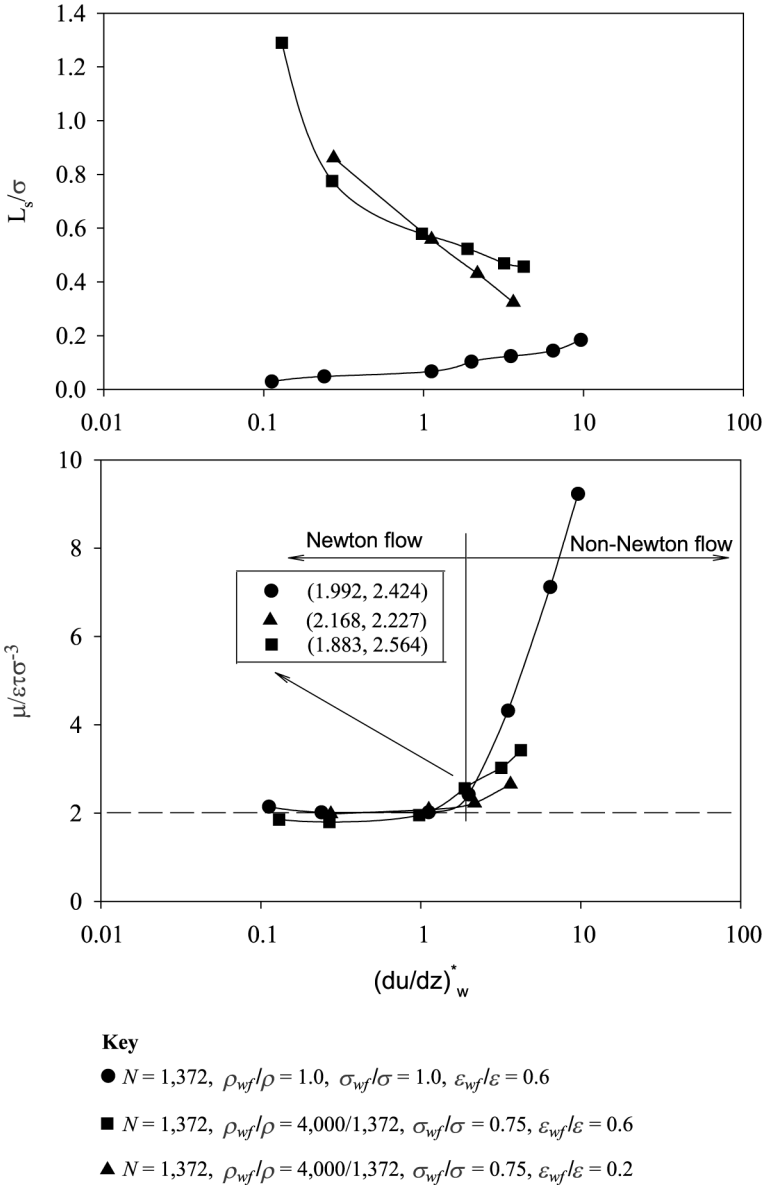

Figure 10.
Slip length and viscosity versus shear rate

The non-dimensional slip lengths and viscosities are shown in Figure 13 versus the non-dimensional shear rate for 500 and 1,372 liquid number system, respectively. Even though the different liquid number system could have different amplitudes of the velocity profiles across the two channel walls, the slip lengths and viscosities show the similar trend. For both 500 and 1,372

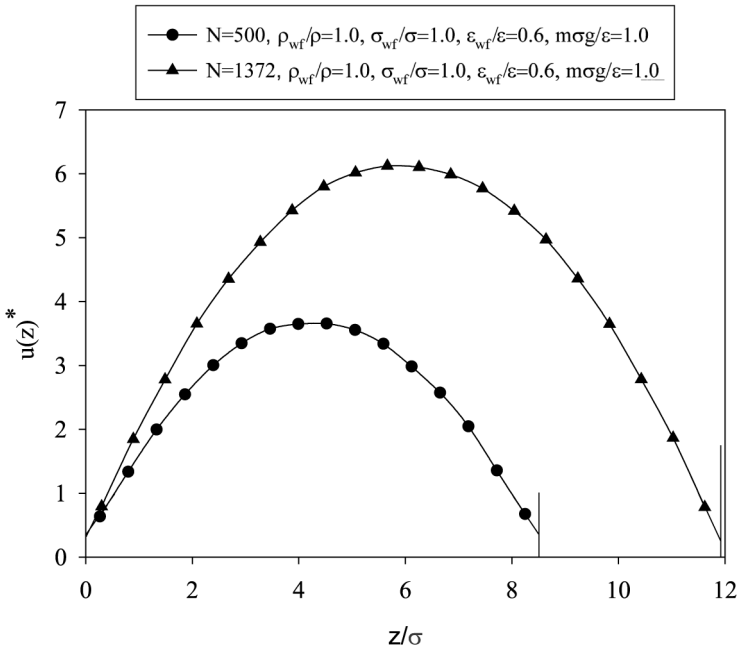

Figure 11.
Effect of molecule number on the velocity profile for strong surface interaction

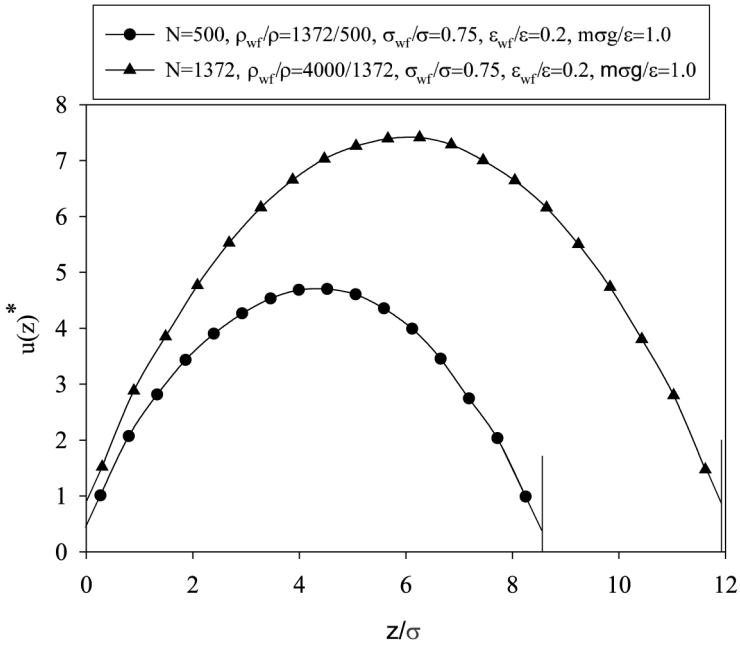

Figure 12.
Effect of molecule number on the velocity profile for weak surface interaction

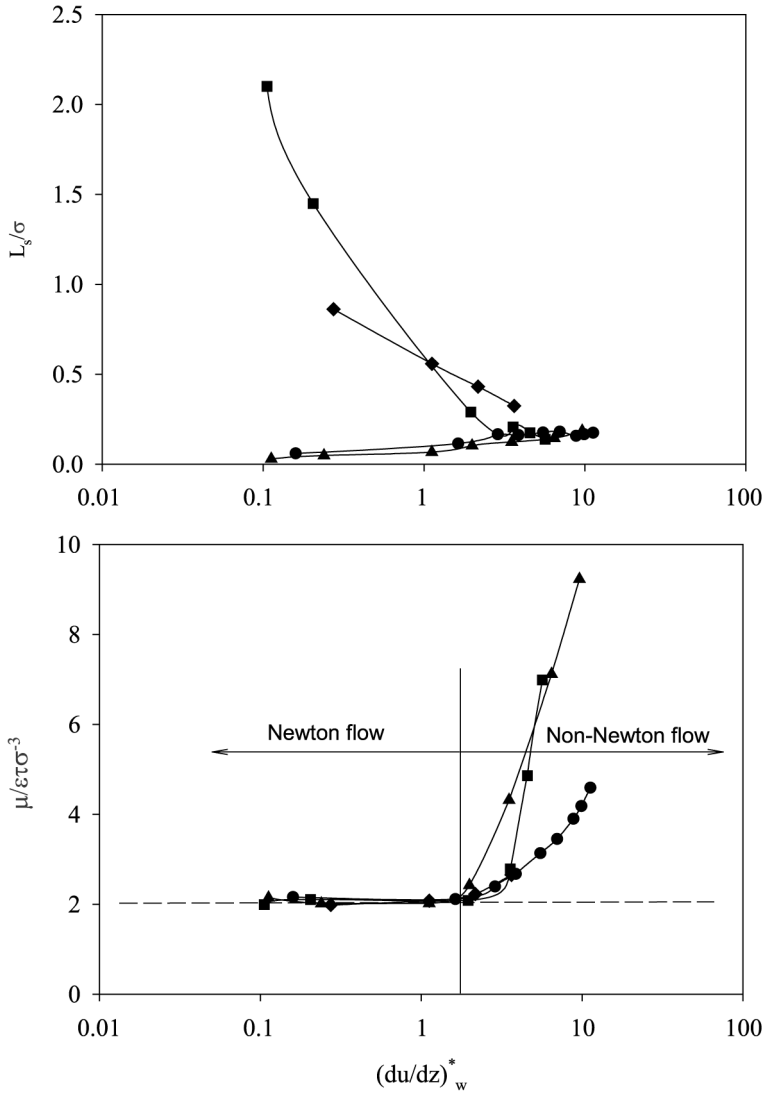

Key

- ● $N = 500$, $\rho_{wf}/\rho = 1.0$, $\sigma_{wf}/\sigma = 1.0$, $\varepsilon_{wf}/\varepsilon = 0.6$
- ▲ $N = 1{,}372$, $\rho_{wf}/\rho = 1.0$, $\sigma_{wf}/\sigma = 1.0$, $\varepsilon_{wf}/\varepsilon = 0.6$
- ■ $N = 500$, $\rho_{wf}/\rho = 1{,}372/500$, $\sigma_{wf}/\sigma = 0.75$, $\varepsilon_{wf}/\varepsilon = 0.2$
- ◆ $N = 1{,}372$, $\rho_{wf}/\rho = 4{,}000/1{,}372$, $\sigma_{wf}/\sigma = 0.75$, $\varepsilon_{wf}/\varepsilon = 0.2$

Figure 13.
Slip length and viscosity versus shear rate for different fluid molecule numbers

liquid number system, the slip lengths are quite small and have a slight increase with increasing the shear rate for the strong fluid/wall interactions. However, the slip lengths are large and dramatically decrease with increasing shear rate for the weak fluid/wall interactions. Again it was observed that the non-dimensional viscosities keep nearly constant of 2.0 when the non-dimensional shear rate is less than 2.0, leading to Newton flow behavior at low shear rate. Beyond the non-dimensional shear rate of 2.0, a transition point from Newton flow to non-Newton flow can be identified obviously. The viscosities have a sharp increase at higher shear rate, leading to the non-Newton flow.

Finally, it is interesting to note from Figures 7 and 8 that the continuum Poiseuille flow solution with the non-slip boundary conditions is the limit of the present MD simulation approaching the very strong fluid/wall interactions. In other words, the liquid approaches to be adhering at the wall surface for the strong fluid/wall interactions (curves dotted by "•" in Figures 7 and 8), leading to the non-slip boundary condition. Under such conditions (continuum Poiseuille flow solution), the liquid particles are being pulled back against the flow direction, thus smaller velocity profiles are obtained than those of the weak fluid/wall interactions.

4. Conclusions

In terms of the present study, the following conclusions can be drawn.

- The micro-Poiseuille flow in nanoscale is successfully modeled by the MD simulation. The flow is activated by applying a uniform gravity force parallel to the channel walls. The model is described in non-dimensional unit system, with the control parameters of the liquid number, the non-dimensional gravity force and the coupling parameters for the fluid/wall interactions.
- The MD simulations were performed over a wide range of non-dimensional gravity forces. It is observed that there are three regions: free molecule oscillation, coupling and gravity force domain regions which have distinct flow behaviors. Such transitions among the regions are strongly dependent on the gravity force and the coupling parameters for the fluid/wall interactions. Strong fluid/wall interactions can sustain a larger coupling region.
- In the coupling region, the non-dimensional number density and velocity profiles are symmetrical about the axial centerline. The number density profiles have a peak value near the wall surface, indicating that the liquid particles are packed much more closely near the wall surface than that far away from the wall. At small gravity forces, stronger fluid/wall interactions lead to a smaller mean axial velocity profile in the channel. At higher gravity forces, the differences of velocity profiles among the strong and weak fluid/wall interactions become smaller.

- For larger liquid number system, the mean axial flow field can be easily established, resulting in a higher velocity profile in the channel.
- For strong fluid/wall interactions, the slip lengths are very small and have a slight increase with increasing the applied gravity force. However, weak fluid/wall interactions lead to higher slip lengths and such slip lengths are dramatically decreased with increasing the shear rate.
- The flow behavior depends on the shear rate. When the non-dimensional shear rate is less than 2.0, the non-dimensional viscosities are nearly constant of 2.0, leading to the Newton flow. Once the non-dimensional shear rate is larger than 2.0, the non-dimensional viscosities are sharply increased with increasing the shear rate and the non-Newton flow appears.

References

Alexander, F.J. and Garcia, A.L. (1997), "The direct simulation Monte-Carlo method", *Computer Simulations*, Vol. 11 No. 6, pp. 588-93.

Gad-el-Hak, M. (1999), "The fluid mechanics of microdevices – the Freeman Scholar lecture", *ASME, Journal of Fluids Engineering*, Vol. 121 No. 5, pp. 5-33.

Haile, J.M. (1992), *Molecular Dynamics Simulation*, Interscience, New York, NY.

Kopiik, J., Banavar, J.R. and Wiiiemsen, J.F. (1989), "Molecular dynamics of fluid at solid surfaces", *Physics Fluids A*, Vol. 1 No. 5, pp. 781-94.

Liem, S.Y., Brown, D. and Clarke, J.H.R. (1992), "Investigation of the homogeneous-shear nonequilibrium-molecular-dynamics method", *Physics Review A*, Vol. 45 No. 6, pp. 3706-13.

Rostami, A.A., Mujumdar, A.S. and Saniei, N. (2002), "Flow and heat transfer for gas flowing in microchannels: a review", *Heat and Mass Transfer*, Vol. 38, pp. 359-67.

Tenenbaum, A., Giovanni, C. and Gallico, R. (1982), "Stationary nonequilibrium states by molecular dynamics – Fourier's law", *Physical Review A*, Vol. 25 No. 5, pp. 2778-87.

Thompson, P.A. and Robbins, M.O. (1990), "Shear flow near solids: epitaxial order and flow boundary conditions", *Physics Review A*, Vol. 41 No. 12, pp. 6830-7.

Thompson, P.A. and Troian, S.M. (1997), "A general boundary condition for liquid flow at solid surfaces", *Letters to Nature*, Vol. 389 No. 25, pp. 360-2.